


# Analysis of damage modes of glass fiber composites subjected to simulated lightning strike impulse voltage puncture and direct high voltage AC puncture

Wenhua Lin<sup>1,2</sup>, Yeqing Wang<sup>1,2</sup> , Youssef Aider<sup>1,2</sup>,  
Mojtaba Rostaghi-Chalaki<sup>3</sup>, Kamran Yousefpour<sup>3</sup>, Joni Kluss<sup>4</sup>,  
David Wallace<sup>3</sup>, Yakun Liu<sup>5</sup> and Weifei Hu<sup>6</sup>

Journal of Composite Materials  
2020, Vol. 54(26) 4067–4080  
© The Author(s) 2020  
Article reuse guidelines:  
sagepub.com/journals-permissions  
DOI: 10.1177/0021998320927736  
journals.sagepub.com/home/jcm



## Abstract

Understanding the damage mechanisms of fiber-reinforced polymer matrix composite materials under high voltage conditions is of great significance for lightning strike protection and high voltage insulation applications of composite structures. In this paper, we investigated effects of the lightning impulse (LI) voltage and high voltage alternating current (HVAC) puncture on damage modes of the electrically nonconductive glass fiber-reinforced polymer (GFRP) matrix composite materials through experimental tests and numerical simulations. The LI and HVAC tests represent the lightning strike and high voltage insulation cable puncture conditions, respectively. Our experimental examinations showed that GFRP composite specimens subjected to the LI voltage test exhibited distinct damage modes compared with those in the HVAC puncture test. The GFRP composite material suffered more charring and fiber vaporization in the HVAC puncture test, whereas less matrix charring and fiber vaporization but severe fiber breakage and delamination in response to the LI voltage tests. The findings indicate that the thermal effect dominates the damage of GFRP composites inflicted by the HVAC puncture test, whereas the mechanical impact effect governs the GFRP composite damage in the LI voltage test. In addition, the electric arc plasma formation during the puncture of the GFRP composite material was modeled through solving Maxwell's equations and the heat generation equations using finite element analysis. Simulation results provided insights on the effects of duration and intensity of the high voltage electric discharge on the composite damage.

## Keywords

Lightning strike, glass fiber epoxy composites, high voltage test, lightning voltage waveform, damage mechanism

## Introduction

High voltage electric discharge, such as lightning strike and high voltage alternating current (AC) direct puncture, poses significant challenges on the material design of lightweight fiber composites for aerospace, renewable energy, modern urban mobility, and electrical insulation cable industries. For example, lightning strike accounts for 23.4% of the wind turbine failure according to the 2012 US wind energy insurance claim report.<sup>1</sup> For a startup commercial wind farm at southwest of the USA, 85% of the wind farm downtime is related to lightning strike and the total lightning-related cost exceeded \$250,000 (in 1997 Dollars<sup>2</sup>). The number

<sup>1</sup>Department of Aerospace Engineering, Mississippi State University, USA

<sup>2</sup>Marvin B. Dow Advanced Composites Institute, Mississippi State University, USA

<sup>3</sup>Department of Electrical and Computer Engineering, Mississippi State University, USA

<sup>4</sup>RISE Research Institutes of Sweden, Sweden

<sup>5</sup>Department of Civil and Environmental Engineering, Massachusetts Institute of Technology, USA

<sup>6</sup>School of Mechanical Engineering, Zhejiang University, P. R. China

### Corresponding author:

Yeqing Wang, Mississippi State University, 501 Hardy Rd, 321 Walker Engineering Building, Mississippi State, MS 39762, USA.  
Email: yw253@msstate.edu

of \$250,000 might seem an insignificant cost, but this could be detrimental for the small start-up wind farms. The fundamental effects of high voltage discharge on fiber composites and metallic materials have drawn growing attention and been investigated by a number of experimental and theoretical studies.<sup>3–26</sup> For instance, numerous studies<sup>3–6,8–15,26–28</sup> have focused on the lightning strike damage of aircraft carbon fiber-reinforced polymer matrix (CFRP) composites. It has been recognized that the Joule heating is the primary cause of the lightning strike damage for CFRP composite panels, and the electrical conductivity played a significant role in the Joule heating generation. Although progress has been made to understand the material behavior and damage mechanisms of the electrically conductive CFRP composites, the findings cannot be directly used to understand those for the glass fiber-reinforced polymer matrix (GFRP) composites, which are electrically nonconductive and still the most widely used structural material for wind turbine blades, civil aircraft, unmanned aerial vehicles, and urban mobility vehicles due to its relatively inexpensive costs as compared to that of the CFRP composites. Due to being electrically nonconductive, the current hardly flows into the GFRP composite material when the high voltage electric arc initially attaches to the material surface. However, when the electric field induced by the lightning strike exceeds the dielectric breakdown strength of the GFRP composite, the dielectric breakdown will occur and instantly form a highly conductive path through the thickness direction of the GFRP composite material. This will produce significant Joule heating along the path, causing puncture or burn through.

Although the GFRP composite material is electrically nonconductive, in many practical applications, it still has a high probability to trigger lightning strikes due to the presence of conductive substances on the material surface, such as moisture, salt, and dust. Moreover, any conductive components inside the GFRP composite structure (e.g. down conductor inside the wind turbine blade) will induce free charges on the material surface. These free charges can easily initiate an upward-connecting leader to arrest the downward-moving stepped leader and form a lightning return stroke.<sup>29</sup> Garolera et al.<sup>30</sup> studied 304 cases of lightning strike damage to wind turbine blades reported from wind farms across the U.S. and observed four primary types of damage due to direct lightning attachment on the blade surface, namely delamination, debonding, shell detachment, and tip detachment. Yokoyama<sup>31</sup> investigated the effects of polluted environments on lightning current discharges on the wind turbine blade surface and found that creeping discharge was only 22.2% of the time for non-polluted blades,

whereas for the polluted blades (with equivalent salt deposit density of  $0.1 \text{ mg/cm}^2$  corresponding to high polluted condition), lightning current creeping discharge was found 100% of the time, and for the worst damaged case, the lightning current punctured through the blade regardless of the embedded down conductors.

The current work studies the effect of the high voltage electric discharge on the nonconductive GFRP composite surface through both lightning impulse (LI) voltage test and high voltage alternating current (HVAC) puncture test, which resembles the lightning strike impulse puncture of the wind turbine blade and high voltage AC direct puncture of an insulation cable, respectively. Here, the lightning strike waveform A voltage was used for the LI voltage test, as suggested by the SAE 5412 standard,<sup>32</sup> shown in Figure 1. It is worth noting that the LI voltage tests are typically used to assess the lightning strike response of electrically nonconductive components, such as the fiberglass skin of a radome, whereas the lightning current waveform with four components used in many existing lightning strike papers is used to assess the lightning strike response of conductive materials, such as the carbon fiber composite materials.<sup>32</sup> The HVAC puncture test was performed in compliance with the IEEE Std. 4-2013<sup>33</sup> and ASTM D149-2009 standards.<sup>34</sup> After the high voltage tests, a detailed examination of the damage zones using ultrasonic scanning and SEM imaging was conducted to characterize the damage mechanisms. Four-point flexural tests were conducted to determine the residual strength of the test specimens. It is worth mentioning that the difference of the breakdown mechanism between the LI voltage test and HVAC puncture test is already widely known to the electrical engineering research community.<sup>35</sup> Hence, this paper is not to provide recommendations on which test needs to be used for studying the lightning strike for GFRP composites, but rather, an attempt to unveil the material response and damage mechanisms

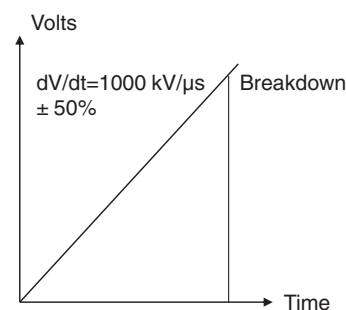


**Figure 1.** Lightning strike voltage waveform A suggested by SAE 5412.<sup>32</sup>

of the GFRP composite material under different high voltage conditions. The understanding gained through this study is expected to provide design guidance on the GFRP composite material for lightning strike protection and other high voltage insulation applications (e.g. insulation cables).

## Experimental systems

### Materials and specimens

The GFRP composite specimens were fabricated by vacuum bagging using the Prepreg 7781 E-Glass purchased from Fibre Glast Developments Corporation. The Prepreg 7781 E-Glass is an 8H Satin Weave prepreg with 30% ( $\pm 3\%$ ) resin. Its density is 1.21 g/cc with a tensile modulus of 2.83 GPa and tensile strength of 79.29 MPa. The layup orientation for the specimens was [+45/-45/0<sub>6</sub>/+45/-45/0<sub>2</sub>]. Such an orientation represents the GFRP composite laminate layup used at the tip region of Sandia 100-meter All-glass Baseline Wind Turbine Blade (SNL 100-00).<sup>36</sup>

The specimens were cured in oven at 310°F for one hour and fifteen minutes. Two 304.8 mm  $\times$  304.8 mm panels were fabricated and then cut in half making four 152.4 mm  $\times$  304.8 mm panels. The four panels will be referred to as Panels 1, 2, 3, and 4, respectively, where Panel 1 is a baseline and was not subjected to any high voltage impacts, Panels 2 and 3 were subjected to HVAC puncture test and Panel 4 was subjected to the LI voltage waveform A test. Note that Panel 2 was bonded with two copper M8 washers on both sides of the panel, while Panels 3 and 4 were bonded with two flat copper electrodes (diameter 50 mm and thickness 25 mm) to comply with the standards. An overview of the test configurations for the four GFRP composite panels is shown in Table 1.

### High voltage test setups

The HVAC test voltage was generated and measured using a Hipotronics AC dielectric test set (model 7100-20A6-F) with rated output of 100 kV and 200 mA.

The LI voltage test was generated by a 2.85 MV, 50 kJ Marx generator. The experimental test setups are shown in Figure 2. Both tests were conducted at the Paul B. Jacob High Voltage Laboratory of Mississippi State University. In the HVAC puncture test, the test voltage across the test sample was increased gradually at a steady rate of 10 kV/s until a disruptive discharge occurred through the panels. The average puncture voltage was observed to be approximately 80 kV. Also, during the LI test, the Marx generator was charged up to 22 kV per stage (i.e. 17 stages) and 0.9 kJ energy approximately discharged through the test sample within a few microseconds. The peak voltage was up to 187.2 kV in the LI voltage waveform A test.

### Specimen preparation

A homogeneous field distribution was achieved by using flat copper electrodes manufactured according to the ASTM D149 standard.<sup>34</sup> The electrodes were adhered to the sample panels using a thin sprayed layer of conductive nickel coat to improve the surface contact conductivity. Moreover, the test samples were immersed in the transformer oil to avoid external flash-over (i.e. surface discharge) occurrence on the surface of panels due to the lower dielectric strength of air as opposed to that of GFRP composite panels (see Figure 3). Figure 3 also shows the setups using both the copper washer electrode and the flat copper electrode. Note that such a test setup was not without its drawbacks. For instance, immersing the GFRP composite panel in transformer oil could have affected the dielectric breakdown strength of the panel due to the absorbance of the transformer oil by the GFRP composite panels. The mechanical properties of the panel could also be affected which have been reported by Amaro et al.<sup>37</sup> where they immersed GFRP composites in various commercial oils and found different levels of strength reduction after the immersion test. The effect of water absorbance may also be useful to assess the deterioration of the composite material under the exposure of transformer oil. For instance, experimental

**Table 1.** High voltage test configurations for the GFRP composite panels.

GFRP composite panel #	Panel preparation	Test configuration
Panel 1	No electrode	Baseline
Panel 2	Two copper washers bonded to both sides	HVAC puncture test
Panel 3	Two flat copper electrodes bonded to both sides	HVAC puncture test
Panel 4	Two flat copper electrodes bonded to both sides	Lightning impulse (LI) voltage waveform A test

HVAC: high voltage alternating current.

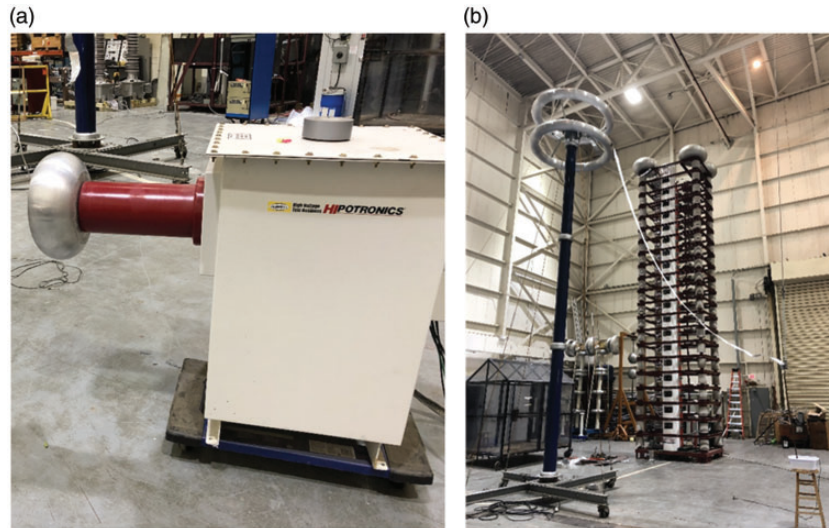


**Figure 2.** The experimental test setups for (a) HVAC puncture test and (b) the LI voltage puncture test at the Paul B. Jacob High Voltage Laboratory of Mississippi State University.

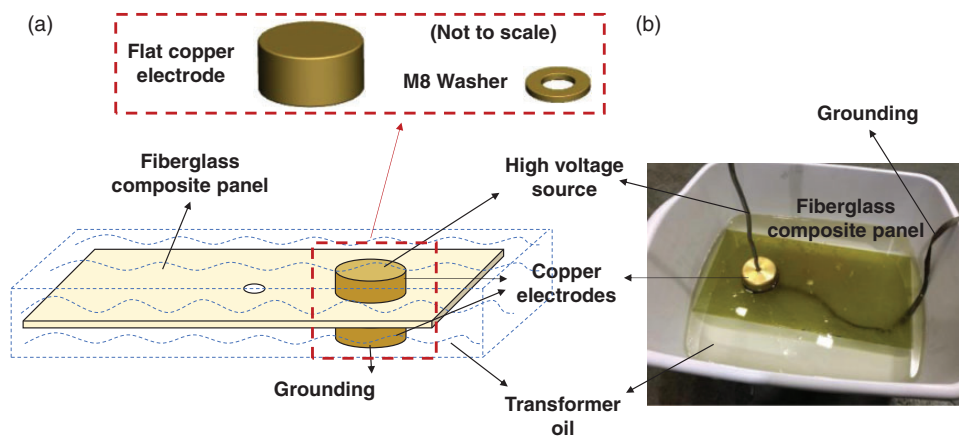


**Figure 3.** (a) Schematic of the GFRP composite panel with electrodes immersing in the transformer oil during high voltage tests and (b) the actual composite panel immersing in the transformer oil.

results indicated that Cyanate Ester/S2 glass composite retains 90% of its dielectric strength after six-month exposure to 99% humidity.<sup>38</sup> Li et al. reported that the residual strength of a carbon fiber epoxy composite panels after lightning strike current impulse test (22 kA peak current) reduced by 5%–20% when the panels were immersed in 60°C water until saturation.<sup>39</sup> Generally, it takes a comparatively long time for the composite material to absorb the moisture and oil before the strength deterioration starts to take effects. In our experimental tests, the total immersion time for our GFRP composite panels during the high voltage tests was less than 20 min. Given such a short time, the effect of the transformer oil on the deterioration of the composite material can be ignored.

### Post-damage material characterization

Ultrasonic inspections and SEM imaging were conducted to examine the damages caused by high voltage tests. The S-scan images were obtained using the OmniScan SX ultrasonic flaw detector from Olympus IMS. The SEM images were obtained using JEOL JSM-6500F Field Emission Scanning Electron Microscope at the Institute for Imaging and Analysis Technology at Mississippi State University. The samples being examined were coated with a thin and uniform layer of platinum to improve the electrical conductivity before SEM imaging. The four-point flexural test in accordance to the ASTM D7264 standard<sup>40</sup> was conducted to determine the



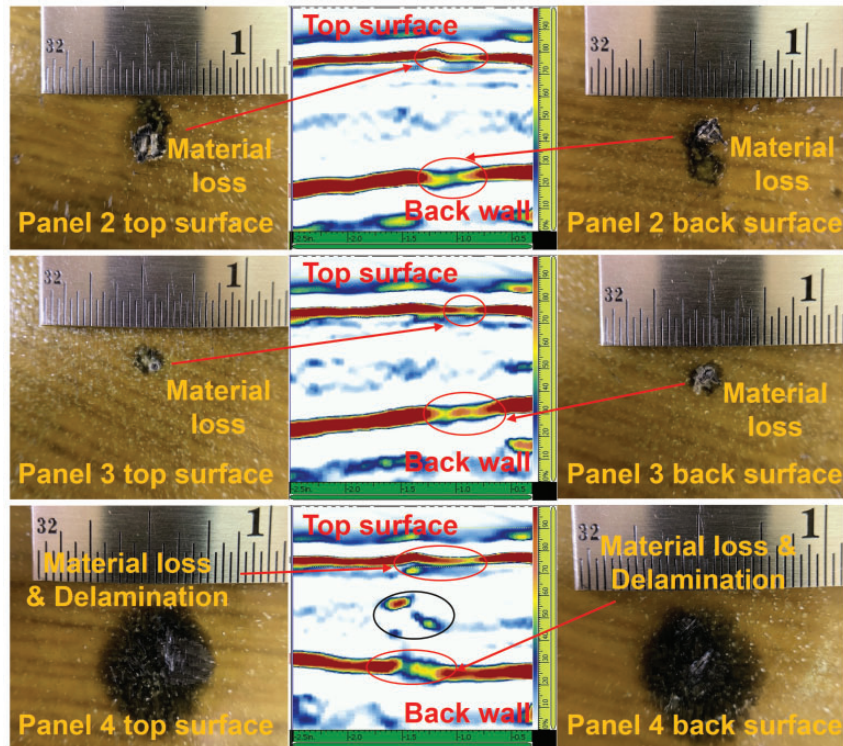


**Figure 4.** (a) Top side high voltage puncture damage of Panels 2, 3, and 4; (b) S-scan images; and (c) bottom side damage.

residual strength of the panels after the high voltage tests.

## Results and discussion

### High voltage puncture damage characteristics

As mentioned earlier, Panels 2 and 3 were subjected to HVAC puncture test, and Panel 4 was subjected to the LI voltage waveform A strike. Note that Panel 2 was bonded with two copper washers on both sides of the panel while Panels 3 and 4 were bonded with two flat copper electrodes to comply with the standards (as shown in Figure 3). For Panels 2 and 3, the average puncture voltage was observed to be approximately 80 kV. Therefore, the dielectric breakdown strength of the GFRP composite panels used in our study is about 30.89 MV/m, which is consistent with those reported by Madsen et al.<sup>41,42</sup> Note that the dielectric breakdown strength can be influenced by the fiber volume fraction and stacking sequence of the composite material. Moreover, various environmental factors, such as the humidity and temperature can also have significant impacts on the dielectric breakdown strength of the composite material.

Visual inspections for both sides of the panels are shown in Figure 4. It can be observed that for all panels subjected to high voltage tests, the damages

were all inflicted near the outermost circumferential regions (within 2.5 mm) of the bonded washer or electrodes rather than at the center or anywhere in between. The electrical field is enhanced at the edge of the electrode (or washer)<sup>43</sup> and hence initiated the damage near the outermost circumferential regions then propagates through the thickness direction with the least resistive path to meet the grounding on the other side of the GFRP composite panel. Here, the least resistive path refers to the path linking to the GFRP composite deficiencies inside the GFRP, which are inevitably introduced during the manufacture process (e.g. voids, resin and fiber non-uniformity). For Panels 2 and 3, which were subjected to HVAC puncture tests, nearly circular puncture holes can be observed along with severe through-the-thickness material losses. For Panel 4, which was subjected to the LI voltage test, much less material loss at the surface can be observed and that the removed material created a highly elliptical shape (about 1.59 mm in longer length) rather than near circular shape by the HVAC puncture test. Moreover, the LI voltage test inflicted much severe delamination within and at the near surface layers of Panel 4. Such damage shapes are similar to the findings of Garolera et al.<sup>30</sup> who studied actual cases of direct lightning attachment damage to wind turbine blades from wind farm reports where they all appear to be long and narrow in shape along with delamination near the

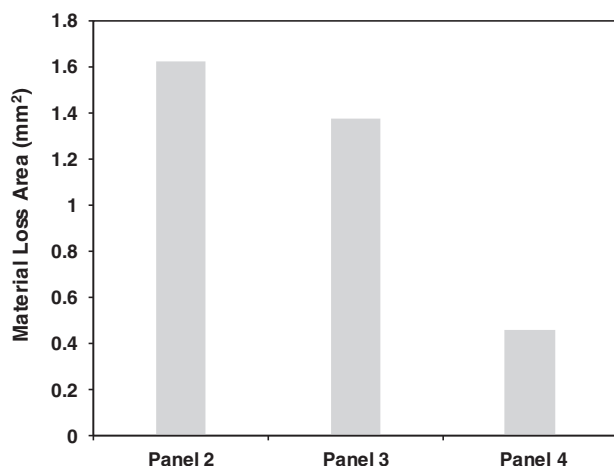


**Figure 5.** Comparison of near surface material loss area for Panels 2, 3, and 4.

lightning attachment point. S-scan images for Panels 2, 3, and 4 shown in Figure 4 further confirmed these visual inspections, the color legend represents the signal amplitude across the detection probe for which strong signal amplitude indicates solidity at the front wall and back surface and lower signal amplitude indicates interlaminar delamination. The Image Processing and Analysis in Java (ImageJ) software was used to quantify the near surface material loss and interlaminar delamination areas of the panels. The material loss area on the GFRP surface integrates areas of the total pixels displaying the complete fiber and matrix material removal. The interlaminar delamination area integrates the areas of the total pixels displaying the black charred areas (i.e. resin fully decomposed, and thus, delamination occurs). The near surface material loss areas for Panels 2, 3, and 4 are 1.625, 1.375, and 0.458 mm<sup>2</sup>, respectively, as shown in Figure 5. The interlaminar delamination areas are 24.121, 11.561, and 133.062 mm<sup>2</sup>, for Panels 2, 3, and 4, respectively, as shown in Figure 6. Given the different bonding materials (washers vs. electrodes) for Panels 2 and 3, it appears that the dimension of the bonding material highly affects the surface material loss and the delamination area. With the smaller dimension of the washer, the electric current flows into the material could be constricted and therefore the current density becomes higher which results in more extensive thermal damage in the GFRP composite.

Figure 7 shows the cross-sections of the GFRP composite panels after the HVAC and LI high voltage experimental tests. As we can see, Panels 2 and 3, which were subjected to HVAC tests, were completely punctured from the top to the bottom surface of the material. They exhibit similar breakdown paths, except that the path in Panel 2 is less straight than that in

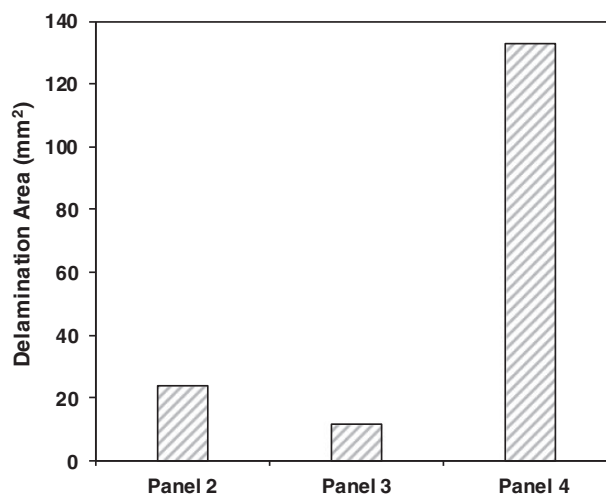


**Figure 6.** Comparison of interlaminar delamination area for Panels 2, 3, and 4.

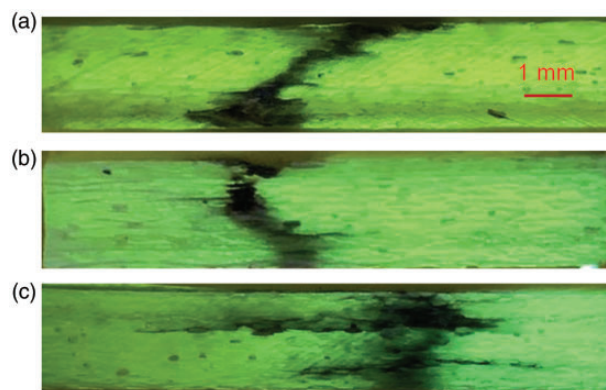


**Figure 7.** Cross-sections of the GFRP composite panels after high voltage experimental tests: (a) Panel 2 after HVAC test; (b) Panel 3 after HVAC test; and (c) Panel 4 after LI test. HVAC: high voltage alternating current.

Panel 3. This difference could be due to the difference in the puncture voltage and the GFRP composite material deficiencies. The puncture diameter for Panels 2 and 3 is in the range of 0.4–0.8 mm. In contrast, Panel 4, which was subjected to the LI test, exhibited distinct damage modes than Panels 2 and 3, where more significant delamination and less material loss can be observed.

It is worth noting that the lightning strike high voltage damage in GFRP composite is quite different from the typical lightning strike damage in CFRP composite, as shown in Figure 8. The difference is due to the different material properties (explained in detail in the SEM imaging section below). As we can see, the CFRP composite shows more extensive damage on the material surface, including delamination, charring, fiber breakage and fiber pullout, and matrix cracking.

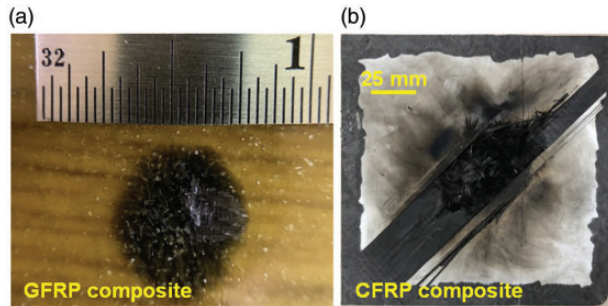


**Figure 8.** Lightning strike damage in (a) GFRP composite (Panel 4 under LI test condition) and (b) CFRP composite (under impulse current with a peak of 100 kV). GFRP: glass fiber-reinforced polymer.

Typically, only top few composite layers will be affected by the lightning strike for CFRP. Direct puncture damage across the entire panel thickness and deep interlaminar delamination, as those observed in our GFRP panels, are not common for CFRP composite and have not been reported.

### SEM imaging

Figure 9 shows the SEM images for Panels 3 and 4 at varying magnification levels. For Panel 3 which was subjected to the HVAC puncture test, the damage appeared to be circular in shape along with extensive amount of matrix vaporization and fiber breakages, whereas for Panel 4 which was subjected to the LI voltage waveform A strike, the damage appeared to be long and narrow which could be explained by the much higher energy level and shorter duration of pulsed current comparing with the HVAC puncture test. Similar damage modes, such as matrix vaporization and fiber breakages, can also be found on Panel 4. In addition to that, matrix cracking was found at the GFRP composite surface and delamination was found at the near surface layers. The circular shape damage for Panel 3 is related to the circular geometry of the electric arc plasma formed when the GFRP is punctured under the HVAC puncture test. When compared to the HVAC test, the LI voltage test requires a much higher voltage to puncture the GFRP ( $\sim 182$  kV vs. 80 kV). With the rapid rising of the electric voltage ( $1000$  kV/ $\mu$ s, see Figure 1), it was initially difficult to puncture the GFRP composite. Instead, it searches for the least resistance path on the material surface to conduct the electric current. Since the electrical conductivity in the fiber direction is higher than that in the through-the-thickness direction (due to interlaminar resin-rich regions), the electric current initially attempts to flow in the fiber direction ( $45^\circ$ , i.e. the orientation of the first ply) on the material surface

before it finally punctured. Therefore, the surface damage on Panel 4 appears to be long and narrow. Such damage has also been reported in many experimental studies for CFRP composites subjected to simulated lightning strike tests.<sup>9,11,14</sup>

Figure 10 shows the SEM images for Panel 3 at the central regions where massive matrix charring and material loss (0.4 mm in radius, 0.8 mm through the thickness) due to fiber vaporization can be observed, and the char residue was deposited at the ends of the broken fibers. The results imply that the damage of the GFRP composite material when subjected to the HVAC puncture is more dictated by the thermal effect, whereas the damage when subjected to the LI voltage waveform A strike is more dictated by the impact effect, potentially due to the shock wave and electromagnetic force produced by the lightning strike. Here, the thermal effect caused by the HVAC puncture for GFRP is different from the thermal effect caused by lightning strike for CFRP. Although both thermal effects are mainly from the resistive heating, the damage mechanisms are different due to the difference between their thermal conductivity ( $0.8$  W/m $\cdot$ °C for GFRP and  $34$  W/m $\cdot$ °C for CFRP in the longitudinal direction at room temperature<sup>19,44</sup>) and electrical conductivity ( $2.17 \times 10^{-16}$  S/m for GFRP and  $3.38 \times 10^4$  S/m for CFRP in the longitudinal direction at room temperature<sup>19,44</sup>). The GFRP is electrically insulating in normal conditions. But when an extremely high voltage (80 kV in HVAC test and 187 kV in LI test) is applied, the dielectric breakdown phenomenon occurs and a conductive path is created to pass through high current density, as shown in Figure 7.

It is worth mentioning that in the breakdown mechanisms of solid dielectrics, the breakdown strength of polymer material decreases significantly with the application time of voltage. The application time in the LI voltage test is much shorter than that in the HVAC puncture test with a step-by-step increasing voltage, which is expected to have a higher breakdown voltage for the glass fiber under the LI voltage test than the HVAC puncture test ( $\sim 187$  kV and 80 kV in our experiment, respectively). The associated breakdown mechanisms are related to the intrinsic breakdown, thermal breakdown, and electromechanical breakdown.<sup>35</sup> These above mechanisms contribute in different levels to the dielectric breakdown of glass fiber caused by the LI voltage test and the HVAC puncture test.

### Residual strength

The four-point flexural test was conducted to determine the residual strength of the specimens after high voltage puncture tests. All four panels were cut down to a width of 88 mm and a length of 300 mm. The support span is



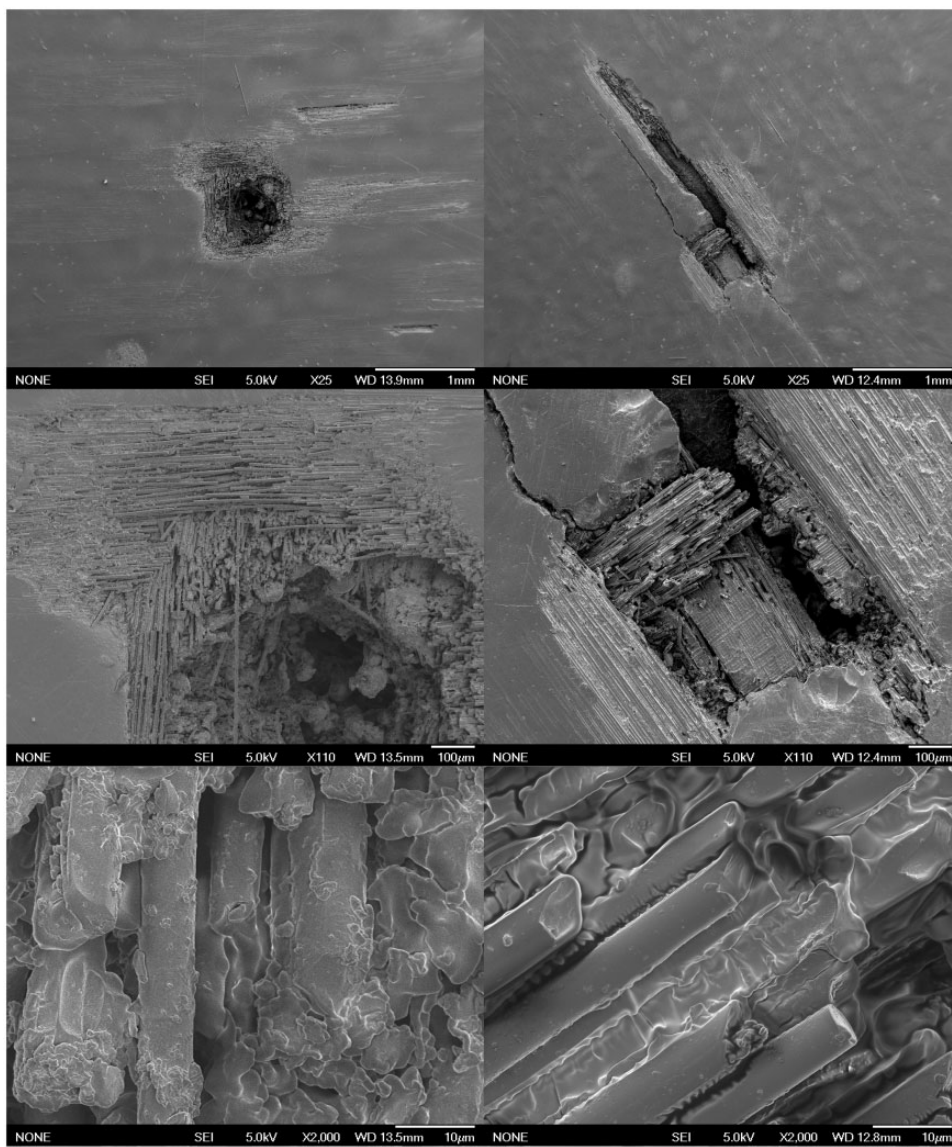


Figure 9. SEM images for (a) Panel 3 and (b) Panel 4 at varying magnification levels.



Figure 10. SEM images for Panel 3 at central region at different magnification levels.



**Table 2.** Computed flexural strength values for the four GFRP composite panels.

GFRP composite panel #	Test configuration	Flexural strength (MPa)	Percentage
Panel 1 (baseline specimen)	N/A	312.13	100
Panel 2	HVAC puncture	>263.31	>84
Panel 3	HVAC puncture	>258.62	>83
Panel 4	LI voltage waveform A	272.14	87

203.2 mm and the load span is 101.6 mm. Table 2 lists the obtained results for the flexural strength. Note that during the flexural test, only Panels 1 and 4 were taken to failure (i.e. complete fiber breakage at the notched center), and the flexural strength are calculated to be 312.13 MPa and 272.14 MPa, respectively.). Panels 2 and 3 were not taken to complete failure even when the panel center touches the top surface of the support fixture and the two over-hang sides start to touch the bottom surface of the load fixture. Given the maximum applied load, the flexural strengths for Panels 2 and 3 are calculated to be 263.31 MPa and 258.62 MPa, respectively, bearing in mind that the actual flexural strength is expected to be higher than the calculated results, hence the “>” sign in Table 2. This implies that the residual strength of the GFRP composite specimen struck by the LI voltage strike is smaller than that of the specimen struck by the HVAC puncture, under conditions used in our tests. In other words, the LI voltage strike could potentially cause more strength loss to the GFRP composite specimen when compared to HVAC puncture test. It is worth noting that the energy flowing into the GFRP composite material in the LI voltage and HVAC puncture tests are different under the test conditions we considered. Therefore, further systematic studies will need to be carried out to investigate the damage mechanisms and strength degradations under test conditions where the electrical energy can be measured and controlled.

It is also worth mentioning that, in this study, one specimen was tested for each high voltage testing condition. It is conceivable that the test results will be affected by the non-uniformity of the specimens due to manufacturing uncertainties, such as the air porosity and non-uniformity of resin and glass fiber. While the variations of the high voltage test results for GFRP composite panels are not available, the variations of the lightning strike test results for CFRP composites are available in the literature and could be useful to assess our specimen variations. For example, Kawakami<sup>26</sup> performed lightning strike tests using two to three composite specimens for each lightning strike testing condition and found that the damage depth of T700/2510 carbon fiber cross-ply composite laminates varied in the range of 3%–8% and the

damage area varied in the range 2%–30% under each lightning strike electric charge transfer level.

## Numerical simulations

To provide a better understanding on the high voltage puncture damage mechanisms of the GFRP composites, numerical simulations were performed by modeling the electric arc generation in the GFRP composite material through solving Maxwell’s equations and the heat energy balance equation using finite element analysis (FEA) with COMOSL Multiphysics. The computational domain is two-dimensional (2D) and 5 mm long and 2.83 mm thick, representing the high voltage-affected region of the GFRP composite panel. Furthermore, the domain is assumed to be axisymmetric due to the near quasi-isotropic laminate schedule of the composite. A surface current density boundary condition with a Gaussian-shaped distribution is assigned to the top surface of the composite material, representing the voltage source. Such a boundary condition has also been used to model tungsten inert gas electric arcs.<sup>45</sup> Here, it should be mentioned that it will be more realistic to apply a voltage boundary condition to resemble the actual high voltage testing condition. However, solving Maxwell’s equation and the heat conduction equation using the high voltage boundary condition gave numerical convergence issues and was unable to model the formation of the electric arc. Therefore, in this study, a current source was assigned instead of the voltage source as a simplification of the problem. The input current source would be able to provide equivalent voltage outputs. The bottom surface of the composite material is grounded. A schematic of the problem setup is shown in Figure 11. Here, the electric arc plasma is analyzed by taking into account the dielectric breakdown and the Joule heating response of the material, and solved in a multiphysics coupling system consisting of the heat energy transfer process and the charge conservation. Both the electrical and thermal conductivities in the material domain are as the function of temperature, offering a pathway to the formation of a conductive route due to the continuous high voltage infliction and the rising temperature response in the lightning–material interactions. The conductive thin path is expected to form throughout

the material's cross section based on our experimental results (see Figure 7) and consistent with the results of Garolera et al.<sup>30</sup> for the damage patterns. The high voltage and its resultant electric field force the minute defects inside the material to breakdown first and momentarily free bound electrons in the following multiple partial breakdown processes. The final result is to forge a conductive path from the top surface of the panel to the grounded bottom surface. The initial electrical conductivity of the GFRP was  $2.17 \times 10^{-16}$  S/m in the through-the-thickness direction and  $1.35 \times 10^{-11}$  S/m in the longitudinal direction.<sup>19</sup> The material properties of the electric arc plasma in the GFRP composites, such as the thermal conductivity, specific heat, and density have not been reported to the authors' knowledge. Here, they are assumed to increase with the temperature following the gradients of the temperature-dependent material properties of the plasma produced in the argon environment,<sup>46</sup> bearing in mind that the species (i.e. electron, ion, neutron) composition of

the plasma produced in the argon and in the vaporized GFRP composite could be quite different. Due to the lack of material properties and uncertainty in the material properties, the simulation presented here should not be considered as a full representation of the aforementioned high voltage experimental tests, but rather, a preliminary attempt to understand the effect of high voltage test parameters, i.e. the current intensity and duration, on the plasma generation and the damage of the composite material. The computational domain is meshed with 10,472 quad elements. The average computational time is about one hour on a laptop with dual core and 16 GB RAM.

### Effect of electric current intensity

The simulation results for the temperature of the electric arc plasma in the GFRP composite panel at three different electric current levels, 50, 100, and 200 A, are shown in Figure 12. Here, the simulations with three current levels are used to investigate the effect of elevated voltage levels on the high voltage puncture damage of the GFRP composite. The duration of all simulations is  $1 \mu\text{s}$ . As one can see in Figure 12, an electric arc plasma is formed between the top and bottom surfaces of the GFRP composite panel for all cases. The maximum temperature of the plasma reached  $3.86 \times 10^4$ ,  $3.05 \times 10^4$ , and  $3.02 \times 10^4$  K at current levels of 50, 100, and 200 A, respectively. The glass fiber evaporates at a relatively low temperature level of 3000 K.<sup>47</sup> It is assumed that the glass fiber is completely vaporized and the gases produced can be ionized to form a plasma discharge in the effect of the extremely high voltage.<sup>3</sup> The plasma temperature is fairly uniform in the axial direction from the top to the bottom with an exception of the 50 A case, where the plasma temperature appears to be concentrated at the top surface

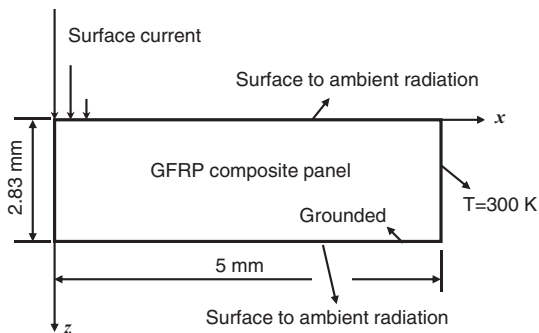


**Figure 11.** A schematic of the problem setup for the numerical simulation (not to scale).

GFRP: glass fiber-reinforced polymer.

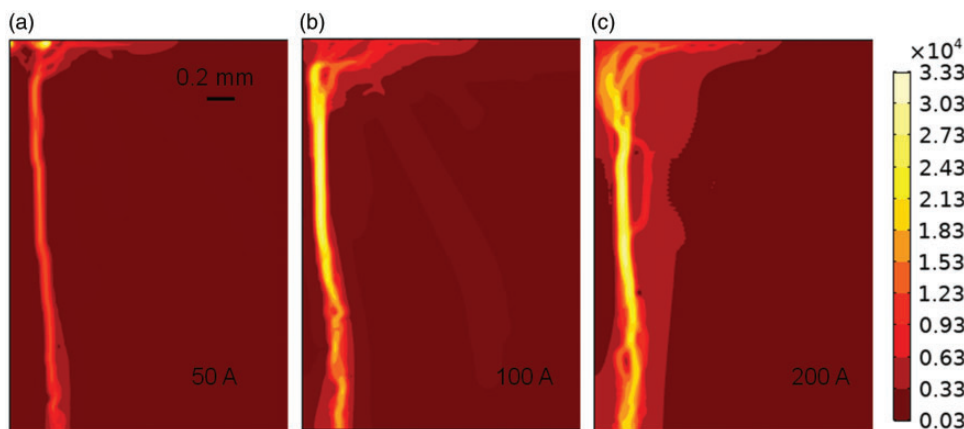


**Figure 12.** The temperature (unit in K) of the electric arc plasma formed in the GFRP composite due to the high voltage puncture at  $1 \mu\text{s}$  and at current levels of (a) 50, (b) 100, and (c) 200 A.

and does not propagate through the thickness. This implies that the puncture through the thickness becomes difficult as the current (or voltage) level decreases. A 3D representation of the electric arc plasma generated in the GFRP composite panel is obtained through revolution of the 2D solution about the  $z$  axis and shown in Figure 13. It can be noticed that the plasma in the GFRP composite forms an approximate hollow cylindrical shape. The radii of the hollow cylindrical channels are 0.35, 0.28, and 0.22 mm. Here, the radius is taken as the distance between the center of the plasma channel (where maximum temperature occurs) and the  $z$  axis. It appears that when the current level increases, the cylindrical plasma gradually converges to the  $z$  axis. If the discharge duration is sufficiently long, the hollow cylindrical plasma channel converges and becomes a solid plasma channel through

the thickness of the composite (see results in the next section). Due to the strong ionization, the material in the plasma channel is presumed to be completely vaporized, leaving a puncture in the composite panel. Moreover, the extreme high temperature from the plasma also leads to matrix decomposition in the regions adjacent to the plasma channel, which results in the deposition of the carbon residue at the ends of the broken fibers. With a hollow cylindrical plasma channel obtained from the current simulations, a ring-shaped puncture is expected to be observed (see Figure 13). However, our experimental examinations from the high voltage tests found either a circular shape or an elliptical shaped material loss (see Figure 9). This inconsistency implies that the discharge duration could be larger than  $1 \mu\text{s}$  (see results in the next section) and/or the actual current could be much higher than 200 A. At the same time, in addition to the material

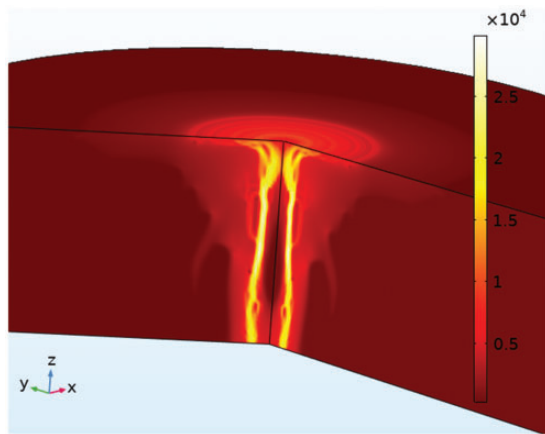


**Figure 13.** A 3D representation of the electric arc generated in the GFRP composite panel at 200 A and  $1 \mu\text{s}$  (temperature unit in K).

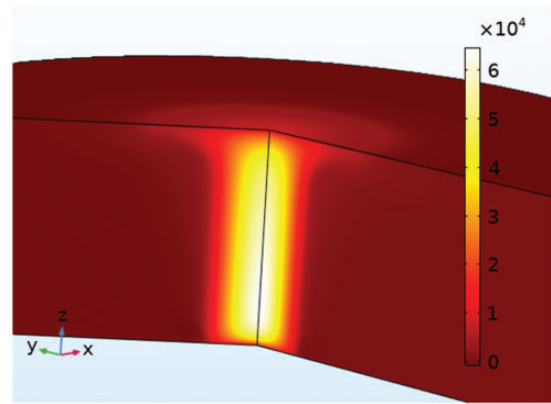


**Figure 15.** A 3D representation of the electric arc generated in the GFRP composite panel at 200 A and  $100 \mu\text{s}$  (temperature unit in K).

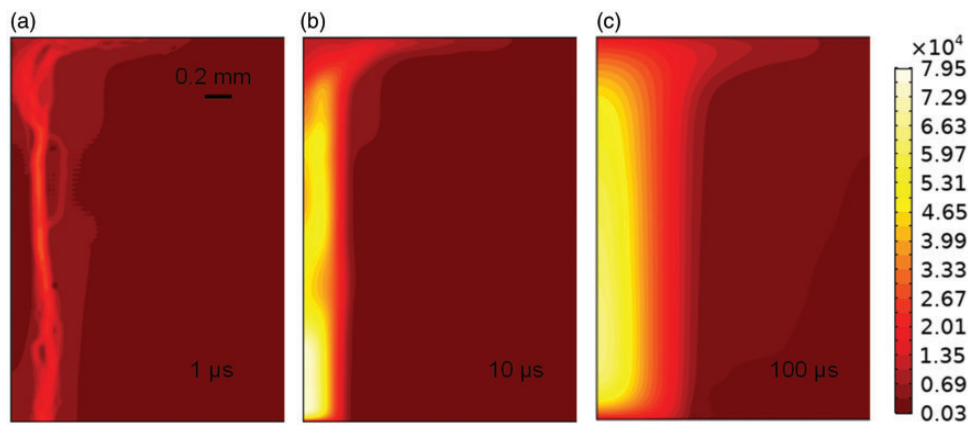


**Figure 14.** The temperature (unit in K) of the electric arc plasma formed in the GFRP composite due to the high voltage puncture at 200 A and with durations of (a) 1, (b) 10, and (c)  $100 \mu\text{s}$ .



vaporization and matrix recession, the high voltage puncture also causes a large area of delamination as evidenced by our experimental tests (see Figure 5). The delamination of the composite could be caused by the electromagnetic force and the acoustic shock wave, which was not predicted from our model and will be a topic of our future work.

### *Effect of electric discharge duration*

Additional simulations were carried out to investigate the effect of the current duration on the electric arc plasma formation and the composite puncture damage. Figure 14 shows the simulation results for the plasma temperature in the GFRP composite panel at 200 A with durations of 1, 10, and 100  $\mu$ s. It can be seen that the electric arc plasma channel has grown from a hollow cylindrical channel to a solid cylindrical channel when the duration was increased to 10 and 100  $\mu$ s. Figure 15 shows the 3D representation of the electric arc plasma at 200 A and at 100  $\mu$ s. The radii of the solid cylindrical plasma, and hence the puncture sizes, are 0.55 and 0.85 mm at 10 and 100  $\mu$ s, respectively. The predicted puncture sizes agree quite well with our experimental test data for panels tested under the HVAC condition (see Figure 7). Here, the radius is taken as the average distance between the 1700 K isothermal line (i.e. melting temperature of glass fiber) to the  $z$  axis. The simulation results imply that the electric arc plasma starts with a hollow cylindrical shape during the beginning of the discharge and gradually converges to a solid cylindrical shape. As the discharge duration increases, the radius of the solid cylindrical plasma channel and hence the size of the puncture grows. The expansion of the electric arc plasma leads to a larger material loss area (i.e. puncture size), which agrees with our experimental observations where the material loss areas subjected to the long-duration HVAC test are generally larger than that subjected to the short-duration LI voltage test.

### **Conclusion**

This paper studied the effects of the high voltage electric discharge on the damage modes of the electrically nonconductive GFRP composites through LI voltage waveform A and HVAC puncture tests. It has been found that the damage appears near the outermost circumferential regions of the bonded electrode (or washer) due to the electric field enhancement effect at the edge of the electrodes. The experimental results also showed that damage mechanisms of the GFRP composite are dependent on the type of high voltage tests. HVAC puncture tests with comparatively longer

duration and lower peak voltage results in more through-the-thickness material loss and excessive charring residuals, while the LI voltage waveform A test with shorter duration and higher peak voltage results in deep interlaminar and near surface delamination along with less through-the-thickness material loss, under the test conditions we used. Moreover, the LI voltage waveform A strike can potentially cause more strength loss to the GFRP composite material than the HVAC puncture test. Our experimental results imply that the damage inflicted by the HVAC puncture is mainly governed by thermal effects, whereas the damage inflicted by the LI voltage waveform A strike is mostly dominated by the impact effects. In addition to experimental tests, numerical simulations with FEA have also been performed to investigate the effects of current intensity and duration on the electric arc plasma formation and the damage to the GFRP composites. The simulation results showed that the electric arc plasma starts with a hollow cylindrical shape and gradually grows to a solid cylindrical shape. The radius of the plasma and hence the puncture size expands as the discharge duration increases. At the same time, the plasma channel also converges to form the solid cylindrical shape faster as the electric current (or voltage) increases. The plasma temperature is sufficiently high to cause material vaporization within the plasma channel and cause matrix recession in the regions adjacent to the plasma channel.

Note that this study is not to provide a recommendation on which test to use for studying the lightning strike damage for nonconductive composite materials, but rather, to unveil the different material responses and damage mechanisms of the GFRP composites caused by two different types of high voltage conditions, i.e. the HVAC puncture and the LI voltage waveform A tests, which represent the cases for the high voltage puncture of insulation cable and lightning strike puncture of nonconductive composite. The understanding gained through this study can provide guidance on the design of GFRP composite materials for lightning strike protection and other high voltage insulation applications. Future work to be done will include conducting lightning strike voltage tests with voltage waveforms B, C, and D and observe the differences in the damage response under different standard voltage waveforms, as well as developing numerical models to evaluate the delamination of the composite material due to electromagnetic force and shock wave produced during the high voltage puncture.

### **Acknowledgements**

The authors wish to thank Mr. Ross Robertson for assisting with the composite material panel fabrication.

### Declaration of Conflicting Interests

The author(s) declared no potential conflicts of interest with respect to the research, authorship, and/or publication of this article.

### Funding

The author(s) disclosed receipt of the following financial support for the research, authorship, and/or publication of this article: The Bagley College of Engineering at Mississippi State University provided the financial support for this project.

### ORCID iD

Yeqing Wang  <https://orcid.org/0000-0002-5673-9897>

### References

1. GCube top 5 US wind energy insurance claims report. <http://www.gcube-insurance.com/news/gcube-top-5-us-wind-energy-insurance-claims-report/> (2013, accessed May 2020).
2. Kithil R. *Lightning hazard reduction at wind farms*. Washington, DC: American Wind Energy Association, 1997.
3. Abdelal G and Murphy A. Nonlinear numerical modeling of lightning strike effect on composite panels with temperature dependent material properties. *Compos Struct* 2014; 109: 268–278.
4. Dong Q, Guo Y, Sun X, et al. Coupled electrical-thermal-pyrolytic analysis of carbon fiber/epoxy composites subjected to lightning strike. *Polymer* 2015; 56: 385–394.
5. Feraboli P and Kawakami H. Damage of carbon/epoxy composite plates subjected to mechanical impact and simulated lightning. *J Aircraft* 2010; 47: 999–1012.
6. Feraboli P and Miller M. Damage resistance and tolerance of carbon/epoxy composite coupons subjected to simulated lightning strike. *Compos Part A: Appl Sci Manuf* 2009; 40: 954–967.
7. Gou J, Tang Y, Liang F, et al. Carbon nanofiber paper for lightning strike protection of composite materials. *Compos Part B: Eng* 2010; 41: 192–198.
8. Guo Y, Dong Q, Chen J, et al. Comparison between temperature and pyrolysis dependent models to evaluate the lightning strike damage of carbon fiber composite laminates. *Compos Part A: Appl Sci Manuf* 2017; 97: 10–18.
9. Guo Y, Xu Y, Wang Q, et al. Eliminating lightning strike damage to carbon fiber composite structures in Zone 2 of aircraft by Ni-coated carbon fiber nonwoven veils. *Compos Sci Technol* 2019; 169: 95–102.
10. Hirano Y, Katsumata S, Iwahori Y, et al. Artificial lightning testing on graphite/epoxy composite laminate. *Compos Part A: Appl Sci Manuf* 2010; 41: 1461–1470.
11. Li Y, Li R, Lu L, et al. Experimental study of damage characteristics of carbon woven fabric/epoxy laminates subjected to lightning strike. *Compos Part A: Appl Sci Manuf* 2015; 79: 164–175.
12. Muñoz R, Delgado S, González C, et al. Modeling lightning impact thermo-mechanical damage on composite materials. *Appl Compos Mater* 2014; 21: 149–164.
13. Naghipour P, Pineda EJ and Arnold SM. Simulation of lightning-induced delamination in un-protected CFRP laminates. *Appl Compos Mater* 2016; 23: 523–535.
14. Ogasawara T, Hirano Y and Yoshimura A. Coupled thermal-electrical analysis for carbon fiber/epoxy composites exposed to simulated lightning current. *Compos Part A: Appl Sci Manuf* 2010; 41: 973–981.
15. Wang FS, Ding N, Liu ZQ, et al. Ablation damage characteristic and residual strength prediction of carbon fiber/epoxy composite suffered from lightning strike. *Compos Struct* 2014; 117: 222–233.
16. Wang FS, Ji YY, Yu XS, et al. Ablation damage assessment of aircraft carbon fiber/epoxy composite and its protection structures suffered from lightning strike. *Compos Struct* 2016; 145: 226–241.
17. Wang FS, Yu XS, Jia SQ, et al. Experimental and numerical study on residual strength of aircraft carbon/epoxy composite after lightning strike. *Aerosp Sci Technol* 2018; 75: 304–314.
18. Wang Y. Multiphysics analysis of lightning strike damage in laminated carbon/glass fiber reinforced polymer matrix composite materials: a review of problem formulation and computational modeling. *Compos Part A: Appl Sci Manuf* 2017; 101: 543–553.
19. Wang Y and Zhupanska OI. Lightning strike thermal damage model for glass fiber reinforced polymer matrix composites and its application to wind turbine blades. *Compos Struct* 2015; 132: 1182–1191.
20. Wang Y and Zhupanska OI. Estimation of the electric fields and dielectric breakdown in non-conductive wind turbine blades subjected to a lightning stepped leader. *Wind Energy* 2017; 20: 927–942.
21. Wang Y and Zhupanska OI. Modeling of thermal response and ablation in laminated glass fiber reinforced polymer matrix composites due to lightning strike. *Appl Math Model* 2018; 53: 118–131.
22. Mall S, Ouper BL and Fielding JC. Compression strength degradation of nanocomposites after lightning strike. *J Compos Mater* 2009; 43: 2987–3001.
23. Liu Y, Guha A, Montanya J, et al. Effects of single impulse current and multiwaveform multipulse currents on aluminum alloy in lightning damage analysis. *IEEE Trans Plasma Sci* 2020; 48: 1146–1153.
24. Liu Y, Fu Z, Liu Q, et al. Experimental and analytical investigation on metal damage suffered from simulated lightning currents. *Plasma Sci Technol* 2017; 19: 125301.
25. Liu Y, Fu Z, Liu Q, et al. Numerical inversion analysis on front-face temperature rise of Al alloy suffered from long continuing current in lightning. *IET Sci Measure Technol* 2018; 12: 467–471.
26. Kawakami H. *Lightning strike induced damage mechanisms of carbon fiber composites*. Washington: Aeronautics and Astronautics Dept. University of Washington, 2011.
27. Sun J, Yao X, Xu W, et al. Evaluation method for lightning damage of carbon fiber reinforced polymers subjected to multiple lightning strikes with different combinations of current components. *J Compos Mater* 2020; 54: 111–125.

28. Wolfrum J, Schuster TJ and Körwien T. Effects of heavy lightning strikes on pristine and repaired carbon composite structures. *J Compos Mater* 2017; 51: 3491–3504.
29. Holbøll J, Henriksen M and Sørensen T. Interaction between electrical discharges and materials for wind turbine blades-particularly related to lightning protection. Denmark: Ørsted DTU, Electric Power Engineering, The Technical University of Denmark, 2007.
30. Garolera AC, Madsen SF, Nissim M, et al. Lightning damage to wind turbine blades from wind farms in the US. *IEEE Trans Power Delivery* 2014; 31: 1043–1049.
31. Yokoyama S. Lightning protection of wind turbine generation systems. In: *7th Asia-Pacific international conference on lightning*. Chengdu, China: IEEE, 2011, pp.941–947.
32. Committee AEL. Aircraft lightning environment and related test waveforms. *SAE ARP A* 2013; 5412.
33. IEEE. IEEE Std 4-2013 (Revision of IEEE Std 4-1995). *IEEE standard for high-voltage testing techniques*. New Jersey: IEEE, 2013.
34. ASTM D149-09. Standard test method for dielectric breakdown voltage and dielectric strength of solid electrical insulating materials at commercial power frequencies. West Conshohocken, PA: ASTM, 2009.
35. Ieda M. Dielectric breakdown process of polymers. *IEEE Trans Electric Insulat* 1980; 206–224.
36. Griffith DT and Ashwill TD. The Sandia 100-meter all-glass baseline wind turbine blade: SNL100-00. Report No SAND2011-3779. Albuquerque: Sandia National Laboratories, 2011, p.67.
37. Amaro AM, Reis PNB, Neto MA, et al. Effect of different commercial oils on mechanical properties of composite materials. *Compos Struct* 2014; 118: 1–8.
38. Morgan B, Madhukar M, Walsh J, et al. Moisture degradation of cyanate ester/S2 glass composite insulation systems. *J Compos Mater* 2010; 44: 821–837.
39. Li Y, Li R, Huang L, et al. Effect of hygrothermal aging on the damage characteristics of carbon woven fabric/epoxy laminates subjected to simulated lightning strike. *Mater Des* 2016; 99: 477–489.
40. ASTM D7264. *Standard test method for flexural properties of polymer matrix composite materials*. West Conshohocken, PA: ASTM International, 2007.
41. Madsen SF, Holbøll J and Henriksen M. Direct relationship between breakdown strength and tracking index of composites. In: *IEEE international symposium on electrical insulation*. Toronto, Ontario, Canada: IEEE, 2006, pp.51–55.
42. Madsen SF, Holbøll J, Henriksen M, et al. Breakdown tests of glass fibre reinforced polymers (GFRP) as part of improved lightning protection of wind turbine blades. In: *IEEE international symposium on electrical insulation*. Indianapolis, IN, USA: IEEE, 2004, pp.484–491.
43. Hsu T-H, Lue H-T, King Y-C, et al. Physical model of field enhancement and edge effects of FinFET charge-trapping NAND Flash devices. *IEEE Trans Electron Dev* 2009; 56: 1235–1242.
44. Wang Y and Zhupanska OI. Thermal ablation in fiber-reinforced composite laminates subjected to continuing lightning current. In: *57th AIAA/ASCE/AHS/ASC structures, structural dynamics, and materials conference*. San Diego, USA, American Institute of Aeronautics and Astronautics, pp.1–17. DOI: 10.2514/6.2016-0986.
45. Hsu KC, Etemadi K and Pfender E. Study of the free-burning high-intensity argon arc. *J Appl Phys* 1983; 54: 1293–1301.
46. Boulos MI, Fauchais P and Pfender E. *Thermal plasmas: fundamentals and applications*. Berlin: Springer Science & Business Media, 2013.
47. Kokkinos D, Gailly P, Georges MP, et al. Real-time measurement of temperature variation during nanosecond pulsed-laser-induced contamination deposition. *Appl Opt* 2015; 54: 10579–10585.